On the application of the forming limit diagrams for quality control of blanks for wheelbarrow of ASTM A1008 carbon steel

Celso Cruz-González[a], Benjamín Vargas-Arista[b], Iván León-Méndez[c], Isidro Guzmán-Flores[d],*

[a] Centro de Ingeniería y Desarrollo Industrial Gerencia de Construcción Mecánica. Ingeniería Mecánica. Av. Playa, Av. Pie de la Cuesta No. 702, Desarrollo San Pablo, 76125 Santiago de Querétaro, Qro., México

[b] Tecnológico Nacional de México, Instituto Tecnológico de Tlalnepantla, Depto. Metal Mecánica, Av. Instituto Tecnológico s/n, Col. La Comunidad, Tlalnepantla de Baz , Estado de México, C.P 54070, México

[c] Centro de Ingeniería y Desarrollo Industrial Sede Querétaro. Av. Playa, Av. Pie de la Cuesta No. 702, Desarrollo San Pablo, 76125 Santiago de Querétaro, Qro., México

[d] Facultad de Sistemas, Universidad Autónoma de Coahuila. Unidad Arteaga, Arteaga, Coahuila, 25350, México

(*Corresponding author: isidroguzman@uadec.edu.mx)

ABSTRACT: The effectivity of the forming limit diagrams in manufacturing wheelbarrow by deep-drawing is shown because of the high material scrap rate which reduces productivity. Several chemical, mechanical testing and microstructural analysis were performed to examine sheet quality and their impact on these diagrams. Chemical analysis revealed that Steel 1 and Steel 3 sheets fulfilled the specification without assuring adequate forming process. However, the higher titanium content of Steel 2 improved its formability since it promoted the formation of fine precipitates, thus refining the grain size. This steel had the highest ASTM grain size number G (9.11), which is the lowest average grain size (13 μm) compared to the other steels, which had G values in the range 8.7 to 9.11. Moreover, Steel 2 sheets had the greatest plastic strain ratio (rm = 1.80), the highest strain-hardening exponent (n = 0.250), the lowest anisotropy Δr = 0.31), yielding better results in deep-drawing strain distribution, the highest forming limit strain (28%) and the highest uniform elongation zone, favoring that failure sites did not occur.

KEYWORDS: ASTM A1008 carbon steel; Forming limit diagram; Plastic strain ratio; Quality control; Strain-hardening exponent

RESUMEN: *Sobre la aplicación de diagramas de límite de conformado para control de calidad en muestras de carretilla de acero al carbono ASTM A1008.* La efectividad de los diagramas de límite de formado en la fabricación de carretillas por embutido profundo es demostrada por el alto desperdicio de material, el cual reduce la productividad.

Se realizaron varias pruebas químicas, mecánicas y análisis microestructural para examinar la calidad de la lámina y su impacto sobre estos diagramas. El análisis químico revelo que las láminas de acero 1 y acero 3 cumplieron la especificación sin asegurar un proceso de formado adecuado. Sin embargo, el mayor contenido de Ti de acero 2 mejoró la formabilidad ya que este promovió la formación de precipitados, refinando el tamaño de grano. Este acero presento el mayor número de tamaño de grano G ASTM (9.11), el cual es el más bajo tamaño de grano promedio (13 μm) comparado con los otros aceros, los cuales tenían valores de G en el rango de 8,7 a 9,11 Además, las láminas de acero 2 tuvieron la más grande relación de deformación plástica ($r_m = 1,8$), el más alto exponente de endurecimiento por deformación (n = 0,250), la menor anisotropía $\Delta r = 0,31$), cediendo mejores resultados en la distribución de deformación en embutido profundo, la más alta deformación límite de formado **(**28%) y la más alta zona de elongación uniforme, favoreciendo que los sitios de fractura no ocurrieran.

ORCID ID: Celso Cruz-González (https://orcid.org/0000-0001-7620-9052); Benjamín Vargas-Arista (https://orcid.org/0000-0002-8210-9186); Iván León-Méndez (https://orcid.org/0000-0003-4756-1246); Isidro Guzmán-Flores (https://orcid.org/0000-0002-1171-8291)

1. INTRODUCTION

An important event occurred in the history of sheet metal forming technology was the publication of an article related to new a criterion for predicting the press performance of deep-drawing sheets, which revolutionized both the philosophy and practice of sheet metal forming in all aspects (Pearce, 1982). In this latter work, the work hardening capacity of sheet steel is accurately reflected by the strain-hardening exponent (*n*) value containing in Eq. (1) from ASTM E646 (2016), that is of major importance in stretching operations. Secondly, a parameter called plastic strain ratio (*r*) determined by Eq. (2) as per ASTM E517 (2000).

$$\sigma = k\varepsilon^n \qquad (1)$$

where: σ = true stress (MPa); k = strength coefficient (MPa); ε = true plastic strain; *n* = strain-hardening exponent

$$r = \frac{\varepsilon_w}{\varepsilon_t} \qquad (2)$$

where: ε_w = true width strain; ε_t = true thickness strain; *r* = plastic strain ratio

The *r* and *n* values are well known as the responsible of almost all forming operations, because *r* is a representation of tensile-compressive strain, while *n* represents the amount of tensile-tensile (biaxial) strain (Drittler and Gricus, 1978; Hursman, 1978; Rolf and Patrick, 1978). Both values as well as the uniform elongation are plotted in the forming limit diagram (FLD), which is a plot of the combination of strains that lead to failure. It is determined experimentally by means of a grid of circles or squares printed photographically on a sheet metal, which were lightly etched. Usually, the circles are 2.54 mm in diameter, however smaller ones may be used. Alternatively, strains can be measured by speckle photography without contacting the specimen, as reported by Hosford and Caddell (2011).

Since the failure of most stamping operations occurs due to localized necking through the sheet thickness, such operations shall be done under quality control. Newby (1978) proposed a set of tensile mechanical testing to prevent the aforementioned failure. In addition, this author explains that yielding locus obey the Von Misses failure criterion and it applies during metal forming. Finally, FLD is a representation of major strains for n ($\varepsilon_1 + \varepsilon_2 = n$), *r* values ($\varepsilon_2 > 0$) and it is a useful tool to predict failures in the manufacturing workshop. Efforts to predict the anisotropy and formability by mechanical tests for 3004-H19 and 5352-H19 alloys were carried out by Lege (1978). The results of fracture angle θ = 68 to 53° and *r* =1.5 to 0.3 agree well with the numerical model. It means that when *r* values decreased, the θ angle was also reduced in the tensile test specimens. On the other hand, 2036-T4 and 5184-O alloys do not agree well with the predictions of the numerical model because of the localized necking occurred. However, the author proposed a correction factor ($\theta_c = 2.48 + 4.9t$) related to sheet thickness (t), achieving an adequate correlation after the correction.

Sipos *et al.* (1995) evaluated the relationship of the *n* and *r* values, as well as crystallographic texture, with the amount of strain during the deep-drawing of a steel sheet (0.047 % C, 0.25 % Mn, 0.19 % Si, 0.022 % Al, 0.017 % V, 0.009 % P, 0.005 % S) of 0.8, 1.0 and 1.4 mm in thickness. This steel yielded *n* ranged from 0.20 to 0.29 at 90° from rolling direction. The results changed depending this direction, a reduction of 7 to 24% was noted when this direction changed from 0 to 90°. The same trend was noted for the *r* values. Erichssen cup testing was performed and then a FLD was plotted concluding that the diagram was useful to predict sheet thinning before the manufacturing schedules. Kohara (2005) investigated the influence of a two-stage strain path on the forming-limit curve (FLC) in sheets of 1.0 mm in thickness of AA1050-O aluminum alloy. The mechanical properties of the studied alloy were 78 and 72 MPa of ultimate tensile strength (σ_u), 0.27 and 0.23 for *n*, and 0.63 and 0.69 for *r* values for the longitudinal and transverse directions, respectively. Limit strains were determined by a circular grid of 2.54 mm in diameter, photographically printed on the surface of the

test blank. The conventional strain was used in the graphs of the FLC that represented the uppermost limit without necking. The results suggested that tensile stress followed by biaxial tensile increasing the forming-limit strains in the region of biaxial tensile deformation.

Barbosa *et al.* (2009) performed an investigation of the formability in AA1100-O aluminum alloy sheets of 0.6 and 0.7 mm in thickness. The mechanical testing included tensile and cup tests in standardized specimens stretched at various strains levels. The results consisted of the FLC for each alloy sheet thickness giving an improvement in formability as the sheet thickness increased. Another research by Korhonen *et al.* (2009) studied the forming and fracture limits of AISI 304 stainless steel and AA3104 aluminum alloy. The yield and ultimate tensile strengths for AA3104 alloy were 277 and 298 MPa respectively, while they were 241 and 610 MPa for 304 stainless steel. Hydraulic bulge testing was employed in the stretch forming experiments. Marciniak-type in-plane and tensile testing were carried out to study the limit strains in the deep-drawing region. Screen-printed and laser-marked grids were used to measure the surface strains. The results indicated that localized necking is responsible to determine the forming limit during stretching for both alloys. So, the theory of Marciniak and Kuczynski may not predict correctly the actual limit strain for such alloys.

For Tisza and Kovács (2012), the FLD is the most appropriate tool to characterize the formability of sheet metal because of the continuous increasing demand of lower consumption and lesser CO_2 emissions, resulting in the need for a weight reduction in automobiles. In this regard, the use of high strength steels is required, so formability testing should be carried out to obtain allowable strain limits since an increment in the thickness, increases the formability of high strength steel sheets. Finally, Shinge and Dabade (2018) performed an experimental investigation on FLD of mild carbon steel. Trials were carried out on grids of circles of 5 mm diameter and samples of 200×200 mm. The major and minor strains of all the ellipses of sheet metal samples stretched at different loads of 12, 14, 16, 18, 20 and 23 kN were calculated. For plotting the FLD, they have selected the ellipse from each sample having maximum strain. Results showed that the area within the curve represented the critical region where the sheet is likely to develop the necking and the onset of failure.

The aim of this work is to prove the effectivity of the FLDs in the manufacturing of deep-drawing metallic forms prior to the forming operations, since some failures can occur within specification steel sheets promoting costly process adjustments and quality testing measurements such as tensile and chemical testing. However, such tests are unable to explain the reason for the failure. Then, specific formability testing such as the FLD could be necessary to explain the phenomenon. FLD was made from Erichssen cup testing results under biaxial stretching at 0, 45 and 90° with respect to the rolling direction using uniaxial tensile testing specimens for tensile-compressive strains. Three suppliers of steel were tested to characterize their stress and strain behaviours, chemical composition and microstructure. Three FLD were plotted by following the ASTM E2218 (2015) procedures for tensile testing and Erichssen cup. Blanks were formed by the deep-drawing process and their strains were plotted against their respective FLD in order to compare formability and introduce a quality control based on the FLD, including circle grid analysis.

2. MATERIALS AND METHODS

Three different ASTM A1008 (2010) deep-drawing carbon steel (DDS) sheets were tested in order to obtain their FLDs, as well as their mechanical properties, microstructural and chemical analysis. Sheet identification was as Steel 1, Steel 2 and Steel 3 for three sheet coupons that were formed by deep-drawing process to verify their performance in forming by means of circle grid analysis.

2.1. Optical emission chemical analysis of steel

Three ASTM A1008 (2010) carbon steel sheets of 1000 mm in length, 1000 mm in wide and 0.90 mm in thickness were chemically analyzed using spectrometric analysis as stipulated in ASTM E415 (1999) standard. Then, test samples of 50×50×0.90 mm³ for each testing coupon were prepared and five randomized tests were performed upon each specimen surface. Afterwards, the average was obtained and compared against ASTM A1008 (2010) standard.

2.2. Microstructural characterization

For metallographic preparation, 10×10×0.90 mm³ test transversal samples were taken from the three carbon steel sheets. The specimens' cross section was mounted and grounded according to ASTM E3-11 (2017) procedure. After final polishing by diamond paste of 1 μm, every test specimen was chemically attacked by using Nital (1% nitric acid and alcohol) to reveal the microstructural features. Light optical observations were carried out with a Nikon optical microscope (OM). All cross section observations were performed at a magnification of x500.

2.3. Tensile mechanical testing

In order to determine the mechanical properties of the three DDS sheets, longitudinal standard tensile test pieces were machined by triplicate according to the ASTM E8 (2016) guidelines. Tensile specimens were tested in an electromechanical Instron 4482 machine with a load cell of 100 kN. Two strain rates were programed; one corresponded to the yielding rate (8 MPa s⁻¹) and a second using a tensile rate of 20 mm

min-1. The specimens' cross section was measured by means of a micrometer with a resolution of 0.001 mm. The extensometer used was a class B-2 Instron with 50 mm gage length with 50% maximum opening, for the yield strength (σ_o) calculation at 0.2% offset.

2.4. Plastic strain ratio and strain-hardening exponent

For the determination of the plastic strain ratio, the strain-hardening exponent, standard tensile testing specimen at 0, 45 and 90° with respect to the rolling direction were machined in triplicate and prepared following the ASTM E517 (2000) and ASTM E646 (2015) guidelines. Tensile specimens were tested in accordance with ASTM E8 (2016) procedure for every orientation. The testing strain range was 5 to 15% and an Instron extensometer with 50 mm gage length was used. The average anisotropy was calculated by Eq. (5) and Eq. (6) from the ASTM E517 (2000) standard.

2.5. Forming limit diagrams (FLD)

The FLD for every Steel 1, Steel 2 and Steel 3 samples of the DDS sheets was constructed by following guidelines in the ASTM E2218 (2015) standard. A hemispherical deformation punch (ball punch test) and uniaxial tensile tests on samples machined at 0, 45 and 90° with respect to the rolling direction were employed to quantitatively simulate biaxial stretch and deep-drawing processes. To obtain the deep-drawing strain, three standard tensile test pieces (for each test coupon) were machined at 0, 45 and 90° with respect to the rolling direction and tested according to the ASTM E8 (2016) standard. Such specimens were marked with circular grids of 2.54 mm diameter using ink. After the specimen's failure, two lectures (90° separated from each one) of the deformed grids (near the necking and next zone) were measured by means of a Nikon OM with a resolution of 0.001 mm and the average was determined.

For the determination of biaxial strain of stretching process, five test specimens of 90×90×0.90 mm³ were prepared including a circle grid marked for every sample of Steel 1, Steel 2 and Steel 3 sheets and tested accordingly to the ASTM A643 (2015) standard. The punch test was performed in a JT Tohsi Inc machine to deform and visible necking occurred around the punch periphery, then stopped experiment was to measure the biaxial deformed grids by means of a Nikon OM and the average was calculated. Finally, the strain plots were constructed according to the ASTM E2218 (2015) standard considering that the first line (strain taken near the necking zone) was the boundary or zone where failure did not occur, but localized necking could be generated. The next line represented a zone of strain taken immediately after the necking zone and was considered as the safe zone of the forming limit.

TABLE 1. Chemical composition results (wt.%) of the Steel 1, Steel 2 and Steel 3 of ASTM A1008 (2010) with Fe to balance

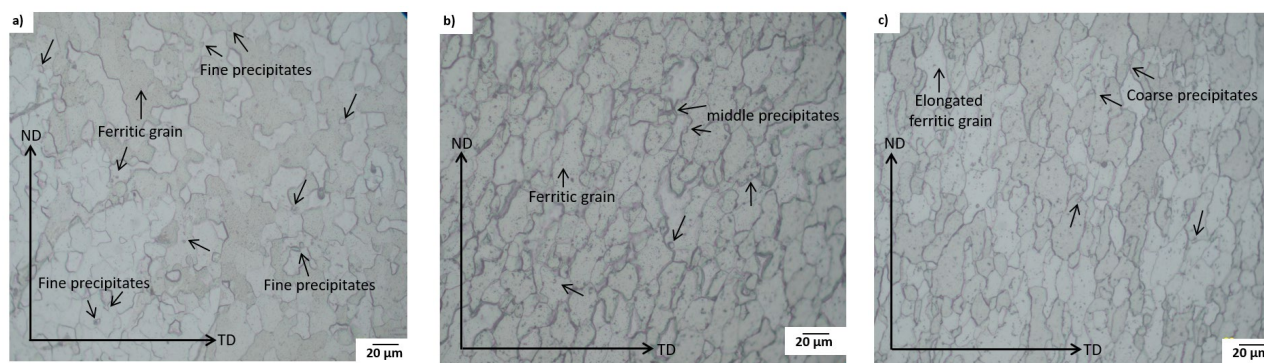| Sheet steel	C	Mn	Si	Ti	Al	P	S
1	0.035	0.1652	0.024	0.0024	0.078	0.008	0.0104
2	0.011	0.1302	0.009	0.0363	0.065	0.010	0.0064
3	0.042	0.1698	0.011	0.0025	0.095	0.009	0.0113
Standard	0.060	0.40	-	0.025	0.01 min	0.020	0.020

FIGURE 1. Optical micrographs at x500 obtained from three DD steel sheets at transversal direction: a) fine precipitates at intragranular sites in microstructure of Steel 2, b) middle size precipitates for Steel 3, and c) coarse precipitates within elongated grains in Steel 1.

2.6. Formability testing on blanks for wheelbarrow

Finally, coupons for the Steel 1, Steel 2 and Steel 3 sheet samples of dimensions 1000×1000×0.90 mm³ were circle grid marked similarly to section 2.5. All steel sheets were lubricated and mounted upon the lower mold installed on a Komatsu hydraulic press of 1000 kN. The lower mold was 2/3 of the dimensions of the press bolster plate and press rate employed was 15 m min⁻¹ (20 spm). After the sheet coupons were formed, two lectures (90° separated of each one) of the deformed grids (near the necking and next zone) were measured using a Nikon OM and the average was reported.

3. RESULTS AND DISCUSSION

3.1. Chemical analysis

Three carbon steel sheets were chemically characterized and the average composition is listed in Table 1 where Steel 1 and Steel 3 fulfilled the ASTM A1008 (2010) standard. Besides, sheet identified as Steel 2 showed the highest titanium content and this could promote precipitation of precipitates containing titanium favoring larger strengthening and hardening. These results were similar to Sipos *et al.* (1995).

3.2. Microstructural analysis

According to the optical microscopy observations undertaken on the three different Steel 1, Steel 2 and Steel 3 sheets, the transverse section microstructures for all samples (Fig. 1) consisted in a ferritic matrix showing mixed grain sizes distribution and orientation with respect to the rolling direction giving elongated grains, containing dispersed and fine precipitates (black points) at mainly intragranular sites and ferrite grain boundaries. The greatest average ASTM grain size number G of 9.11 was achieved for Steel 2 (Fig. 1a), followed by 8.9 for Steel 3 sheet (Fig. 1b) and finally 8.87 with elongated grains for Steel 1 sheet (Fig.1c). The microstructure of Steel 2 showed a slight refinement of the ferritic grain size with an average value of 13 µm (Fig. 1a) compared to the average grain size of

16 µm for Steel 3 (Fig. 1b) and the largest average grain size (19 µm) for Steel 1 sheet, as it can be seen in Fig. 1c.

Regarding to precipitates within the microstructure of three DDS sheets, is clearly observed that higher amount of fine precipitates (indicated by arrows) mainly at intragranular sites was exhibited in Steel 2 (Fig. 1a), followed by Steel 3 sheet containing middle size of precipitates (Fig. 1b), and Steel 1 sheet showed coarse size of precipitates, see Fig. 1c. This precipitate behaviour could be related to the differences in the Ti composition of the steels, as it has been reported a larger amount of Ti in the Steel 2 sheet composition (Table 1). Moreover, cracks were not identified as reported by Sipos *et al.* (1995). Therefore, there were as-rolled ferritic microstructures with differences in grain size and density of precipitates depending of chemical composition of three DD steel sheets. These grain sizes and precipitates' distributions influenced the mechanical behaviour under tension as it is explained in the next section.

3.3. Tensile strength

Figure 2 depicts the tensile mechanical response of Steel 1, Steel 2 and Steel 3 sheets. It is clearly seen that Steel 3 exhibited the highest yield and ultimate tensile strengths compared to the other two steel sheets. The three steels behaved similarly behaviour, i.e., no upper and lower yield strengths, discontinuous yield-
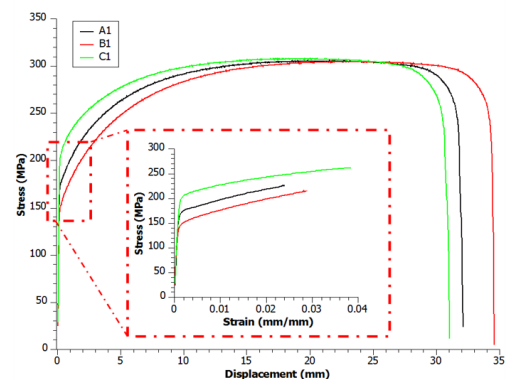

FIGURE 2. Stress vs displacement curves for three steel sheets with the same thickness of 0.9 mm.

TABLE 2. Tensile properties results for three steel sheets

Sheet steel	Yield strength 0.2%, σ_o (MPa)	Ultimate tensile strength, σ_u (MPa)	Elongation at 50 mm (%)
1	167.0 ± 0.4	289.0 ± 1.3	47 ± 0.8
2	171.0 ± 0.5	301.0 ± 0.2	47 ± 0.4
3	191.0 ± 0.1	305.0 ± 0.5	48 ± 0.4
Standard	-	115 to 200	≥ 38

TABLE 3. Values of r_m, Δr and n for three steel sheets

Sheet steel	Average Plastic strain ratio (r_m)	Earing tendency (Dr)	Average strain hardening exponent (n)
1	1.52	0.65	0.230
2	1.80	0.31	0.250
3	1.60	0.52	0.200
Standard	1.4 to 1.8	-	0.200 to 0.250

ing or yield point elongation were observed in the strain-hardening zone, as it can be observed inset plot that focusses on the stress-strain behavior at the lower applied strains. The latter behaviour was reported in the DD steel sheets that were based in same standard, thus a similar manufacturing process was likely performed.

Furthermore, the average of the tensile properties obtained after performing three different tensile test using longitudinal standard tensile specimens is shown in Table 2 for Steel 1, Steel 2 and Steel 3 sheets, which fulfilled the ASTM A1008 (2010) standard where significant differences were noted among the steels. The Steel 3 sheet reached the highest values of σ_u as well as σ_o, which was linked to the greatest weight percentage of C (0.042%) and presence of intragranular precipitates in middle ferritic grain size (16 μm), followed by Steel 2 as a consequence of the largest percentage of Ti (0.0363%) resulting in several intragranular precipitates and grain refinement with values of 13 μm, and Steel 1 sheet that revealed the lowest aforementioned strengths with reduction of 13% in σ_o compared to Steel 3 and similar elongation as Steel 2 sheet, which was related to larger grain size (19 μm) containing lesser amount of precipitates.

3.4. Plastic strain ratio and strain-hardening exponent results

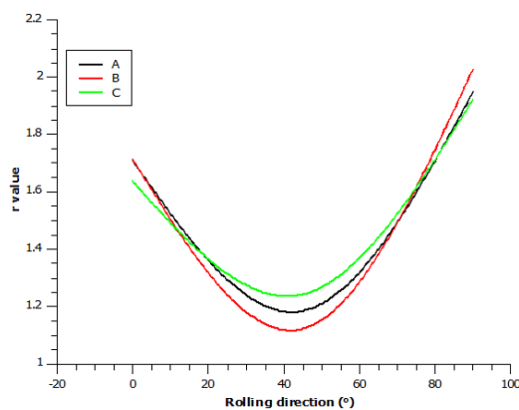The results of the r_m (average of 0, 45 and 90° with respect to the rolling direction), average n values, as well as anisotropy Δr (mechanical properties differs on dependence of steel sheet rolling direction) are shown in Table 3, which were within the expected values reported in the ASTM A1008 (2010) standard. The r_m values were different for three sheets, which suggested that the average mechanical behaviour could be affected. The Steel 1 achieved lesser r_m value (1.52) which was an indicative of the decrement in drawing height operation as well as the deformed necking tendency because strains were higher along the sheet thickness of 0.9 mm (Barbosa *et al.*, 2009). Moreover, the Steel 1 revealed the largest anisotropy ($\Delta r = 0.65$) in comparison to Steel 3 and Steel 2 sheets, suggesting that their lower mechanical properties were non-uniform within

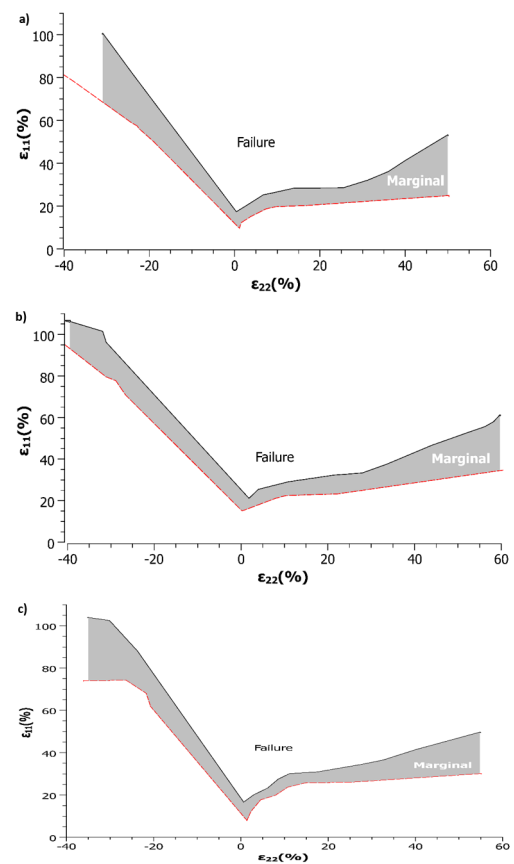FIGURE 3. *r* values as a function of rolling direction for three steel samples.

FIGURE 4. Forming limit diagrams for: a) Steel 1, b) Steel 2, and c) Steel 3.

the sheet in comparison to the other two steel sheets with higher tensile strength and lower Δr, representing a good indicator of lesser tearing tendency (Sipos *et al.*, 1995).

The Steel 3 sheet showed the lowest strain-hardening exponent (n = 0.200) compared to Steel 1 and Steel 2 sheets, which showed larger hardening and
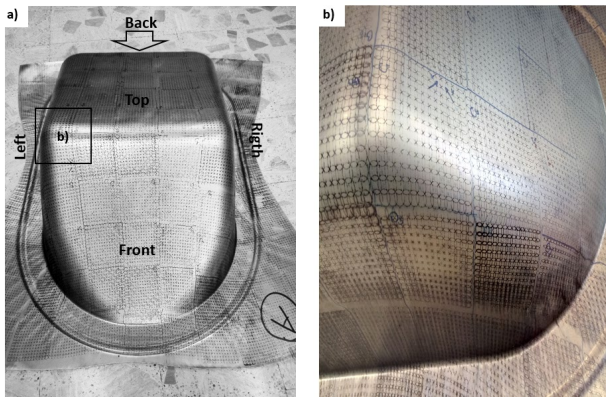

FIGURE 5. Wheelbarrow formed by deep-drawing process: a) upper view, and b) left corner zone from a).
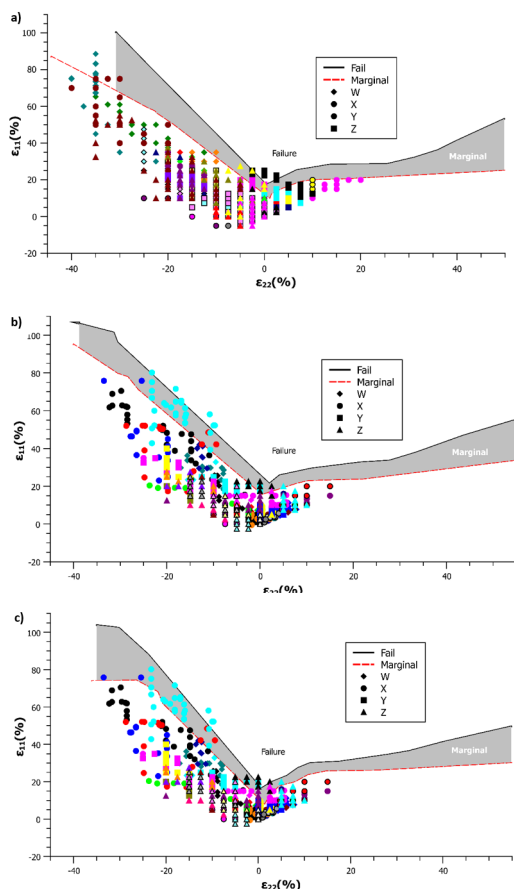

FIGURE 6. Forming limit diagrams for: a) Steel 1, b) Steel 2, and c) Steel 3 showing four strain zones (W, X, Y, Z) within wheelbarrow after deep-drawing process.

strengthening behaviour, resulting in a lesser capacity to strain-harden, i.e., the bi-axial strain would be lower for Steel 1. Therefore, the latter sheet could have a lower height for bulge forming process associated with the plastic strains during forming that surpasses the uniform elongation at lower stress levels. Finally, Steel 2 sheet possessed the best formability under permanent plastic strain as a consequence of the greatest n value (0.250) and the lowest mechanical anisotropy (Δr = 0.31) representing a higher degree of forming strain and hardening response.

The Fig. 3 shows the r values obtained depending of the orientation with respect to the rolling direction (0, 45 and 90°) for three steel sheets. As it can be noted, the greatest values were obtained at 90° of direction for three steels, which was associated with more grain boundaries favoring the plastic deformation. Moreover, Steel 2 sheet reached the highest r value, followed by Steel 1 and Steel 3 sheet which show the lowest values at 90°. This behavior can be explained based on the finer average ferrite grain size of this steel (13 µm) which provides a higher grain boundary density. This finer ferrite grain could be due to the higher amount of Ti in this steel, which would promote a larger amount of precipitates in the matrix, which acted as grain refiner. On the contrary, the lowest r values were found at 45° of the rolling direction for the three steels. This can be explained based on the alignment of the ferritic grains along the maximum shear stress. This is a typical behaviour of the semi-killed steel as reported by Semiatin (2006).

3.5. Forming limit diagrams (FLDs) for Steel 1, 2 and 3 sheets

The Fig. 4 shows the FLDs for three steel sheets where the vertical axis (ε_{11}) represents the transverse strain, while horizontal one (ε_{22}) is the longitudinal strain, according to Hosford and Caddell (2011) and Newby (1978) the behaviour of the sheet metal in uni-axial tension can be used to estimate the performance in other stress states, and this is confirmed by the ASTM E2218 (2015) standard. Right zone on the plots in this figure indicates the tensile and compressive strains resulting in the deep-drawing process limits, as well as tearing tendency. Left area is a representation of the biaxial stretching (tensile-tensile strain) process. Finally, the center line exhibited a uniform elongation zone: 23% for Steel 1 (Fig. 4a) and 28% for Steel 2 and Steel 3 sheets, in accordance to Davis (2004). The Steel 2 (Fig. 4b) reached the highest formability because the forming limit strain was 20%, favored by the largest values of r_m (1.80) and n (0.250) and higher uniform elongation. Besides, Steel 1 and Steel 3 sheets had a similar formability limit strain and a lower value (10%) in comparison to Steel 2. Moreover, Steel 3 (Fig. 4c) depicted the greatest tearing tendency because of the ε_{11} = 75 to 105%, ε_{22} = − 40% and bigger anisotropy Δr value (0.52) compared to the other two sheets.

3.6. Formability results on carbon steel wheelbarrows

The Fig. 5 depicts a wheelbarrow after adequate forming with black inset points representing the zone where the highest strains could occur. It is clearly seen that Fig. 5a reveals a wheelbarrow formed by deep-drawing process where notable wrinkles appeared in the flange zone. In addition, Fig. 5b reveals the strained grids in the edge radius of the wheelbarrow bottom. Moreover, the deep-drawing process was related to the σ_u value as this is the main difference among the Steel 1, Steel 2 and Steel 3 sheets, i.e., the higher σ_u of steel, the larger deep-drawing force needed. Taking into account the force formulae calculation (Semiatin, 2006) for rectangular drawing, the load required to perform the deep-drawing of the Steel 1, Steel 2 and Steel 3 sheets was 229.5, 301 and 305 kN, respectively. Therefore, it is necessary an increment of 31% in load to draw Steel 2, and 33% of more load to draw Steel 3, both compared to the Steel 1 sheet.

Additionally, four zones were analyzed on the wheelbarrow after that deep-drawing process was carried out. Flange zone was marked with letter W and wrinkles were revealed, walls area was identified with X, corner edge zone was marked with Y, and letter Z represented bottom area of wheelbarrow. In Fig. 6, most of the strain zones of the flange and walls of the wheelbarrow corresponded to the bi-directional strain area as a consequence of the deep-drawing process. Moreover, the bottom areas followed the stretching zone mainly because such zone did not stretch significantly during the forming process.

Figure 6a shows the strain distribution of the wheelbarrow manufactured with Steel 1. Some points in the marginal zone and likelihood of failure where noted in the uniform elongation zone ($\varepsilon_{1,1} = 10\%$ and $\varepsilon_{22} = 0\%$). In addition, the majority of strain points where located in the biaxial strain zone (deep drawing area) and were below the safe area. Figure 6b reveals the strain profile of the wheelbarrow manufactured with Steel 2 sheet. Several strain points were located in the marginal zone of the biaxial strain area and few points in the failure zone, suggesting a likelihood failure at the edge zone (Y) linked to local thinning (necking). The latter formability trend was noted for the wheelbarrow manufactured with Steel 3, see Fig 6c.

4. CONCLUSIONS

− In this research it was necessary to perform a lot of testing on materials taken from the real production line, which can be very expensive and represent a high waste of time and money. Therefore, a simple and more effective method to solve such kind of problems is the employment of the forming limit diagrams prior to forming operations because they could help to determine the best metallurgical quality of steel sheet instead of having to undertake several press-die adjustments. The validity of these diagrams in the manufacturing of deep-drawing wheelbarrow was demonstrated by analyzing the chemical composition, the mechanical behavior and the microstructure in three ASTM A1008 steel sheets taken from production batches.

− The Steel 2 sheet showed the highest titanium content which would promote the formation of fine precipitates in the microstructure that could lead to a refinement of the microstructure. This steel shows the highest ASTM ferrite grain size number G (9.11), equivalent to an average ferritic grain size of 13 μm and the larger yield and ultimate tensile strengths in comparison to the other two steels, improving the sheet formability. Moreover, it reached the highest plastic strain ratio ($r_m = 1.80$) as well as the largest strain-hardening exponent (n = 0.250) representing highest capacity for plastic deformation, which was linked to a better uniform elongation zone.

− The Steel 1 sheet exhibited lesser yield and ultimate tensile strengths, linked to the greatest average ferrite grain size of 19 μm which is equivalent to the lowest ASTM number G of 8.87. This steel showed the lowest plastic strain ratio ($r_m = 1.52$), strain hardening exponent of n = 0.230 and the largest anisotropy value ($\Delta r = 0.65$), resulting in lower degree of forming limit strain (10%) and lack of drawing formability.

− Additional deep-drawing parameters measured for Steel 2, such as: the mechanical anisotropy measured, Δr, found to be the lowest (≥ 0.31), the strain hardening exponent, n, to be the greatest (≥ 0.250), the forming limit strain ($\geq 28\%$) and the r_m, which was the highest (≥ 1.80) could be included in the process specifications to reduce forming defects as cracking, tearing, necking and wrinkles.

ACKNOWLEDGMENTS

REFERENCES

ASTM E415 (1999). Standard test method for optical emission vacuum spectrometric analysis of carbon and low-alloy Steel. ASTM International, West Conshohocken, PA, USA, pp. 3-5.

ASTM E517 (2000). Standard test method for plastic strain ratio r for sheet metal. ASTM International, West Conshohocken, PA, USA, pp. 1-5.

ASTM A1008 (2010). Standard specification for steel, sheet, cold-rolled, carbon, structural, high-strength low-alloy, high-strength low-alloy with improved formability, solution hardened, and bake hardenable. ASTM International, West Conshohocken, PA, USA, pp. 1-9.

ASTM E643 (2015). Standard test method for ball punch deformation of metallic sheet material. ASTM International, West Conshohocken, PA, USA, pp. 1-4.

ASTM E2218 (2015). Standard test method for determining forming

limit curves. ASTM International, West Conshohocken, PA, USA, pp. 1-10.

ASTM E646 (2016). Standard test method for tensile strain-hardening exponents (n-values) of metallic sheet materials. ASTM International, West Conshohocken, PA, USA, pp. 2-5.

ASTM E8 (2016). Standard test methods for tension testing of metallic materials. ASTM International, West Conshohocken, PA, USA, pp. 7-18.

ASTM E3-11 (2017). Standard guide for preparation of metallographic specimens. ASTM International, West Conshohocken, PA, USA, pp. 1-8.

Barbosa, J.E., García, I.H., Fuentes, J.J. (2009). Estimación vía experimental de la formabilidad de láminas de aluminio de pureza comercial. *Rev. LatinAm. Metal. Mater.* 29 (2), 128-134.

Davis, J.R. (2004). *Tensile testing*. Second Edition, ASM International, USA, pp. 251-257.

Drittler, O.E., Gricus, F.V. (1978). *Formability of aluminum alloys using cup tests. In Formability topics-metallic materials*. ASTM STP 647, pp. 39-48.

Hosford, W.F., Caddell, R.M. (2011). *Forming limit diagrams. In Metal forming, Mechanics and metallurgy*. Cambridge University Press, Michigan, USA. pp. 245-262.

Hursman, J. (1978). *Development of forming limit curves for aerospace aluminum alloys*. ASTM International, pp. 49-64.

Kohara, S. (2005). Influence of strain path on the forming-limit curve in aluminum. *Metall. Mater. Trans. A* 36, 1033-1037. https://doi.org/10.1007/s11661-005-0296-8.

Korhonen, A.S., Manninen, T., Yoon, J.W., Larkiola, J. (2009). Comparison of forming and fracture limits of an aluminum alloy and austenitic stainless steel. *Int. J. Mater. Form.* 2 (1), 431- 434. https://doi.org/10.1007/s12289-009-0489-6.

Lege, D.J. (1978). *Predicting sheet anisotropy from fracture angle of tension specimens*. ASTM International, pp. 86-99.

Newby, J.R. (1978). *Formability testing and deformation analysis of steel sheet*. Armco Steel Corporation, Middletown, Ohio, pp. 4-38. https://doi.org/10.1520/STP30043S.

Pearce, R. (1982). *4000 years of sheet metal forming*. In *Formability of metallic materials*. ASTM STP 753. Eds., American Society for Testing Materials, pp. 3-18.

Rolf, R.L., Patrick, E.P. (1978). *Bending and spring back of aluminum alloy sheet and plate*. ASTM International, pp. 65-85. https://doi.org/10.1520/STP30046S.

Semiatin, S.L. (2006). *Metalworking: sheet forming (ASM Handbook)*. Volume 14B, ASM International, USA, pp. 524-560.

Shinge, V.R., Dabade, U.A. (2018). Experimental investigation on forming limit diagram of mild carbon steel sheet. *Procedia Manuf.* 20, 141-156. https://doi.org/10.1016/j.promfg.2018.02.020.

Sipos, K., Martínez, J., Burgos, N., Pesenti, H. (1995). Aceros para embutido profundo: fabricación, caracterización, microestructura y texturas. *Rev. Metal.* 41 (Extra.) 58-63. https://doi.org/10.3989/revmetalm.2005.v41.iExtra.999.

Tisza, M., Kovács, Z.P. (2012). New methods for predicting the formability of sheet metals. *Production Process and Systems* 5 (1), 45-54.